The Stolk operator in GPSPI migration

Chad M. Hogan, Gary F. Margrave

ABSTRACT

The Stolk operator is introduced as a replacement for the square-root operator found in traditional GPSPI migration. This operator allows for a transverse (that is, horizontal) slowness gradient, instead of assuming a fully homogenous output location as is the case with GPSPI migration. Some differences in image quality were found for both impulse-response type tests and for Marmousi migration tests. The observed improvements in the image quality are minor, while the computational time costs are relatively extremely high.

INTRODUCTION

Much of the current research in "wavefield extrapolation methods" (WEM) is directed towards improving the quality of the WEM code without sacrificing numerical efficiency. Modern algorithms that make use of WEM, such as the Generalized Phase-Shift-Plus-Interpolation (GPSPI) migration algorithm due to Margrave and Ferguson (1999), have produced high-quality seismic images at affordable computational costs. Moving beyond GPSPI migration will require either significantly better images, or significantly improved numerical performance without a loss of imaging quality (or both). The current GPSPI migration operator uses an approximation in which the local wavefield propagation velocity is assumed to be a constant. We evaluate a new migration operator that mathematically extends the capabilities of the GPSPI operator beyond this assumption to account for a local first derivative in (horizontal) slowness.

Recursive phase-shift wavefield propagation

Many current WEM algorithms are space-frequency methods related to or derived from the phase-shift method introduced by Gazdag (1978). Fourier-transforming the scalar wave equation results in the Helmholtz equation, which results in an interpretation of the wavefield as a sum of plane waves. By applying an appropriate phase-shift to each plane wave, the wavefield may be propagated through a distance accurately.

Generalized PSPI

The GPSPI algorithm is an accurate, efficient implementation of these phase-shift concepts. This algorithm takes an entire constant-depth-slice of the wavefield and propagates it to a deeper level. The z (depth) direction is typically referred to as the *range* direction, while horizontal directions x and sometimes y are referred to as *transverse* directions. In addition to Fourier-transforming the time series of the data, it is often convenient to represent the transverse directions x and y in their Fourier-transformed coordinates, k_x and k_y.

Mathematically, the GPSPI algorithm may be represented in compact operator notation

as:

$$\Psi(x, z = \Delta z, \omega) = \mathbf{T}_\alpha \Psi(x, z = 0, \omega) \tag{1}$$

Or, more explicitly:

$$\Psi(x, z = \Delta z, \omega) \approx \int_{\mathbb{R}} \phi(k_x, z = 0, \omega) \alpha\left(k\left(x\right), k_x, \omega\right) e^{ik_x x} dk_x \tag{2}$$

where

$$\alpha\left(k\left(x\right), k_x, \omega\right) = \left\{ \begin{array}{c} e^{i\Delta z k_z(x)}, |k_x| \leq \frac{\omega}{v(x)} \\ e^{-|\Delta z k_z(x)|}, |k_x| > \frac{\omega}{v(x)} \end{array} \right. , \quad \begin{array}{r} k_z(x) = \sqrt{k(x)^2 - k_x^2} \\ k(x) = \frac{\omega}{v(x)} \end{array} \tag{3}$$

and

$$\phi(k_x, z = 0, w) = \frac{1}{2\pi} \int_{\mathbb{R}} \Psi(x, z = 0, \omega) e^{-ik_x x} dx \tag{4}$$

The algorithm applies a nonstationary filter to the data (Margrave, 1998), is a pseudodifferential operator in the Standard Calculus (Hörmander, 1985) and is the limiting form of the PSPI algorithm described by Gazdag and Sguazzero (1984) when taken to the extreme of using a separate velocity for each and every output point. (Margrave and Ferguson, 1999). In the pseudodifferential calculus, α is known as the symbol of the operator $\mathbf{T}_\alpha$, which is explicitly defined in equation (2).

It may be seen that the wavefield $\Psi(x, z, \omega)$ at each output point $(x_0, \Delta z)$ is the result of the wavefield extrapolation operator $\mathbf{T}_\alpha$ applied to the entire line $(x, 0)$ $x \in \mathbb{R}$. A new operator is constructed for each required output point along the line using the local velocity at the output point $v(x_0, \Delta z)$. The core assumption at the heart of the GPSPI method is its dependence on the fact that the wavefield at each output point $(x_0, \Delta z)$ is calculated by propagating the wavefield from the line at depth $z = 0$ assuming that the entire wavefield at depth $z = 0$ propagates through a medium of constant velocity $v(x_0, \Delta z)$. That is, the local region between the line $(x, 0)$ $x \in \mathbb{R}$ and the point $(x_0, \Delta z)$ is assumed to be homogeneous. For this reason, equation (2) with symbol as defined in equation (3) is often referred to as the locally-homogeneous approximation (Fishman et al., 1997). The magnitude of Δz is typically on the order of $\sim$ $10m$, which is usually much smaller than the scale of the range velocity variation and so a range-homogeneous approximation is often reasonable. In numerical implementations the length of the line $(x, 0)$ $x \in \mathbb{R}$ is frequently many hundreds of meters or more, so a transversely-homogeneous approximation is far from ideal. Dipping events with strong velocity gradients will likely not be imaged accurately.

The Stolk operator

It is hoped that mathematically-sound extensions to the GPSPI migration scheme that allow for locally-inhomogeneous velocity models will result in improved image quality compared to computational cost. We consider the specific case of transverse velocity variations. The hope is that this will allow for high-quality images in media that feature strong lateral velocity variations – salt-dome flanks, for example. This extension of the operator is accomplished by adapting the theory introduced by Stolk (2004) into a new GPSPI-type operator.

The formal mathematical approximations to the solutions of the Helmholtz equation developed by Stolk (2004) form a new operator that may be tested in comparison to the GPSPI operator. This theory is especially attractive as it presents itself as a correction to the standard operator (the "square-root") used in GPSPI migration. Specifically, the Stolk correction adds a term involving the derivative of the slowness s, so that the k_z term within α in equation (3) becomes:

$$k_z(x) = \left(\sqrt{\frac{\omega^2}{v(x)^2} - k_x^2}\right) + \frac{ik_x}{2}\frac{\omega^2}{v(x)}\left(\frac{\partial s}{\partial x}\right)\left(\frac{\omega^2}{v(x)^2} - k_x^2\right)^{-3/2} \tag{5}$$

This means that it is relatively straight-forward to adapt existing GPSPI code to make use of this new operator. Some care must be taken to ensure a valid implementation within fast versions of the GPSPI ideas such as the FOCI algorithm (Margrave et al., 2004) to ensure that the correction is not lost via some assumption (for example, the FOCI method normally assumes a symmetric operator, which the Stolk operator is not).

Equation (5) has one obvious problem: there is a singularity at the evanescent boundary, that is where $\omega/v(x) = k_x$. Stolk (2004) corrects for this by using a damping term $h(\varsigma)$ that masks the singularity:

$$h(\varsigma) = \begin{cases} 0 & \varsigma \leq 0, \\ \exp(-1/\varsigma)/(\exp(-1/\varsigma) + \exp(-1/(1-\varsigma))) & 0 < \varsigma < 1, \\ 1 & \varsigma \geq 1 \end{cases} \tag{6}$$

If we use $v(x)\,|k_x/\omega|$ to define ς, and shape an appropriate function built from equation (6), the resulting damping term effectively removes the singularity but passes the bulk of the wavelike region.

The resulting operator may be displayed in both the $\omega - x$ and $\omega - k_x$ domains. In Figure 1, the Stolk operator for frequency $70Hz$, $v = 2000ms^{-1}$, with no horizontal velocity (slowness) gradient is displayed. This operator is exactly equivalent to the usual FOCI operator for these parameters. Referring to Figure 2, this operator may be directly compared to the Stolk operator for precisely the same medium but with one difference: a local slowness gradient equivalent to a velocity gradient of approximately $35s^{-1}$. Notice the dramatic change in both the $\omega - x$ and the $\omega - k_x$ representations. The operator is clearly asymmetric, reflecting the asymmetric nature of the underlying medium.

The effect is obviously frequency dependent. At low ($15Hz$) frequency, the resulting operator can be seen in Figure 3, and at intermediate frequency ($30Hz$) the operator can be seen in Figure 4. Changing the sign of the velocity gradient also reverses the asymmetry of the operator, as seen in Figure 5, in which the $30Hz$ case is recalculated with an effective velocity gradient of $-4s^{-1}$. Additionally, it can be seen in this figure that a weaker velocity gradient ($-4s^{-1}$ compared to $35s^{-1}$) results in a weaker distortion of the otherwise-flat operator in the $\omega - k_x$ plots.

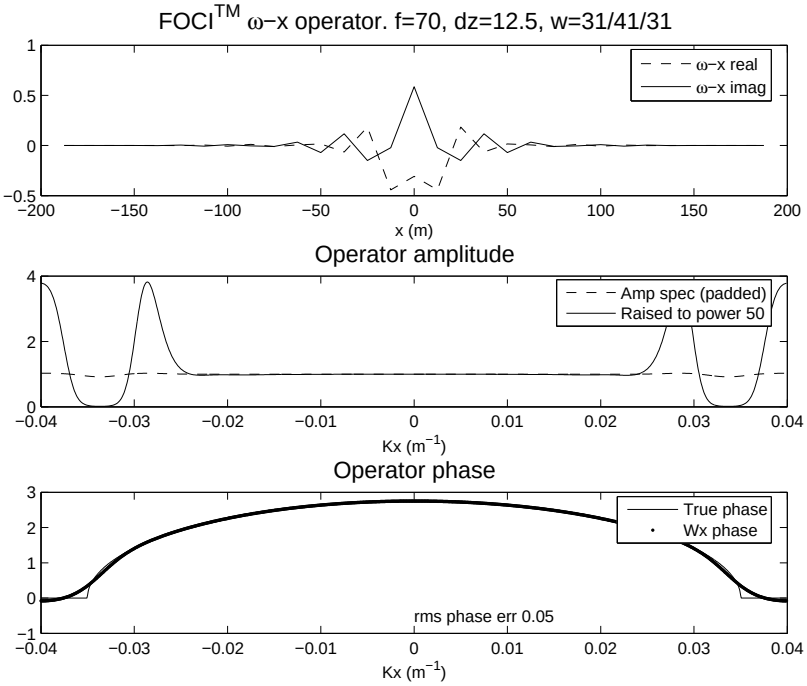

FIG. 1. The Stolk operator in $\omega - x$ and $\omega - k_x$ domain for $70Hz$ at $2000ms^{-1}$ with no horizontal velocity (slowness) gradient – *ie* this operator is exactly equivalent to FOCI. The top panel shows the $\omega - x$ operator, the middle panel shows the operator amplitude in $\omega - k_x$, and the bottom panel shows the operator phase in $\omega - k_x$.

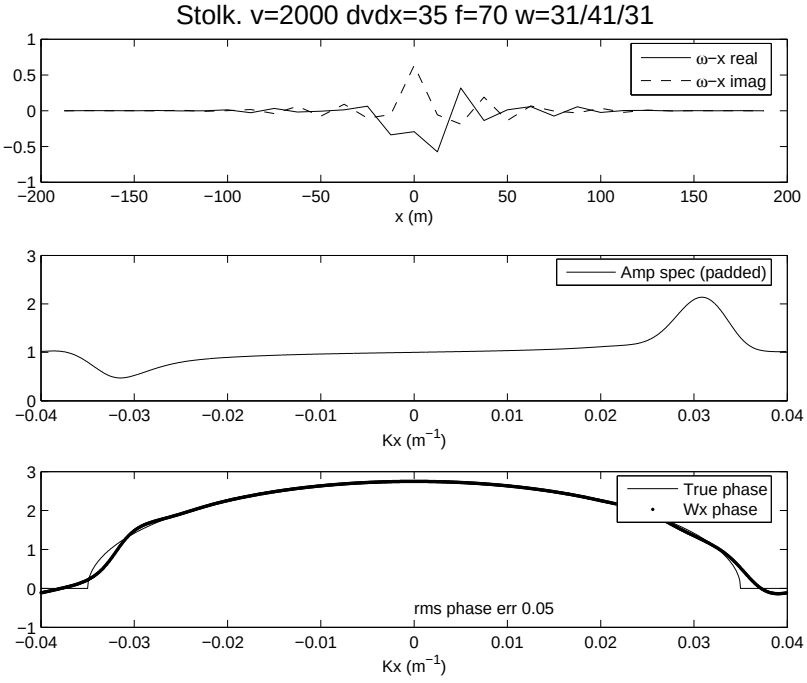

FIG. 2. The Stolk operator in $\omega - x$ and $\omega - k_x$ domain for $70Hz$ at $2000ms^{-1}$ for $35s^{-1}$ velocity gradient. The top panel shows the $\omega - x$ operator, the middle panel shows the operator amplitude in $\omega - k_x$, and the bottom panel shows the operator phase in $\omega - k_x$.

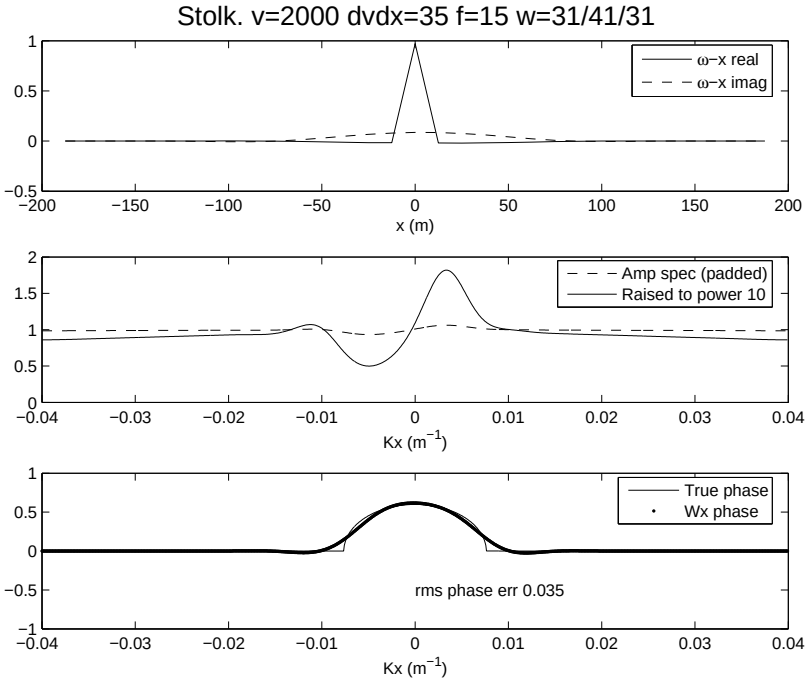

FIG. 3. The Stolk operator in $\omega - x$ and $\omega - k_x$ domain for $15Hz$ at $2000ms^{-1}$ for $35s^{-1}$ velocity gradient. The top panel shows the $\omega - x$ operator, the middle panel shows the operator amplitude in $\omega - k_x$, and the bottom panel shows the operator phase in $\omega - k_x$.

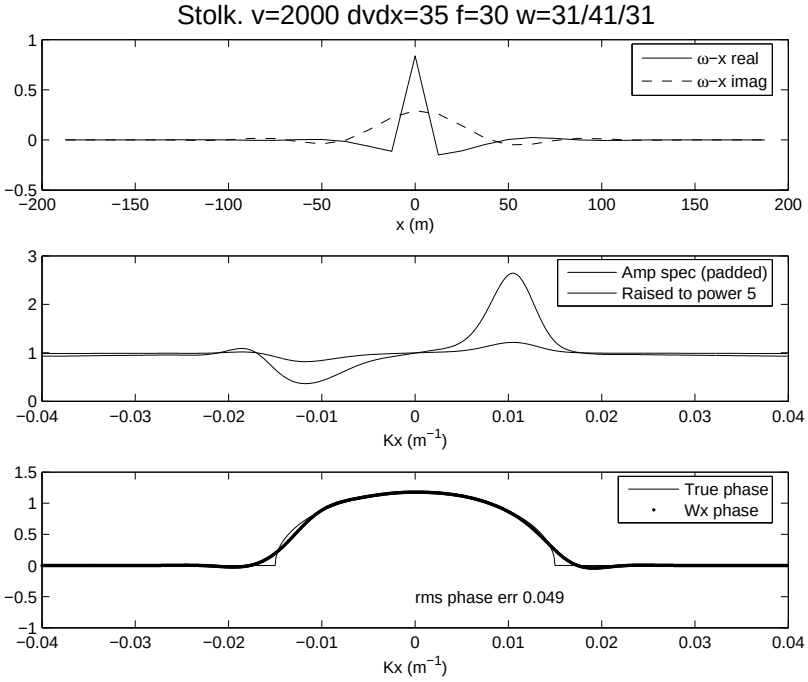

FIG. 4. The Stolk operator in $\omega - x$ and $\omega - k_x$ domain for $30Hz$ at $2000ms^{-1}$ for $35s^{-1}$ velocity gradient. The top panel shows the $\omega - x$ operator, the middle panel shows the operator amplitude in $\omega - k_x$, and the bottom panel shows the operator phase in $\omega - k_x$.

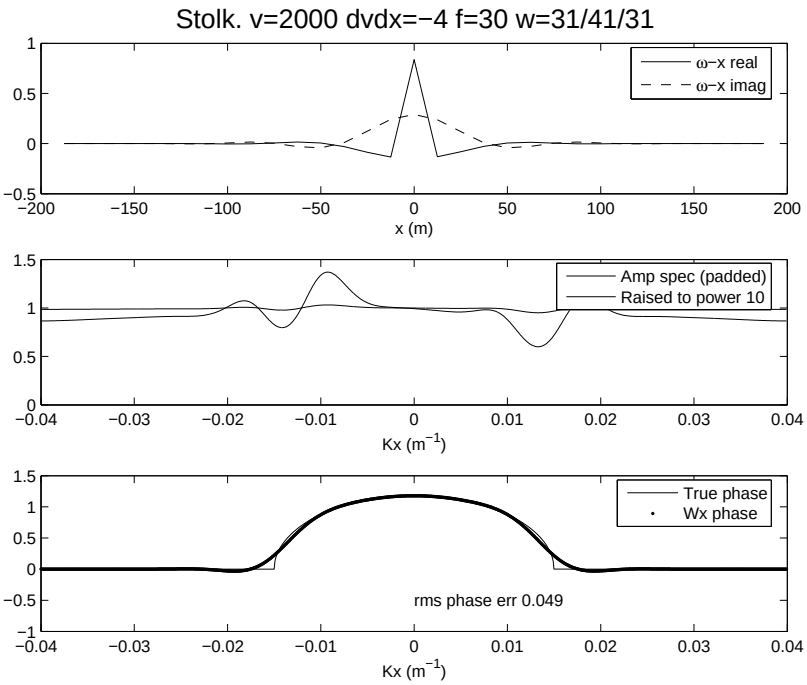

FIG. 5. The Stolk operator in $\omega - x$ and $\omega - k_x$ domain for $30Hz$ at $2000ms^{-1}$ for $-4s^{-1}$ velocity gradient. The top panel shows the $\omega - x$ operator, the middle panel shows the operator amplitude in $\omega - k_x$, and the bottom panel shows the operator phase in $\omega - k_x$.

TESTING

The Stolk symbol was implemented in both the standard GPSPI and FOCI fashion, using existing MATLAB codes developed by CREWES and POTSI. Impulse response and focussing-power tests were calculated using standard GPSPI methods, while full pre-stack depth migrations were calculated using the FOCI algorithm.

Impulse response

The impulse reponse of the Stolk symbol in a homogeneous medium is compared to the standard square-root in Figure 6. The responses are identical in appearance as they should be for a homogeneous medium. They are numerically identical as well. The impulse response of the symbols through an inhomogenous medium, specifically one with a strong horizontal velocity profile, is shown in Figure 7. Once again, the symbols look very similar. The difference, however, is only apparent upon subtraction of the two impulse responses as seen in Figure 8. Overall, the character of both impulse responses is extremely similar. In Figure 7 the strength of both impulses is nearly identical. The Stolk response appears to be somewhat smoother qualitatively, and this makes up the bulk of the difference shown in Figure 8.

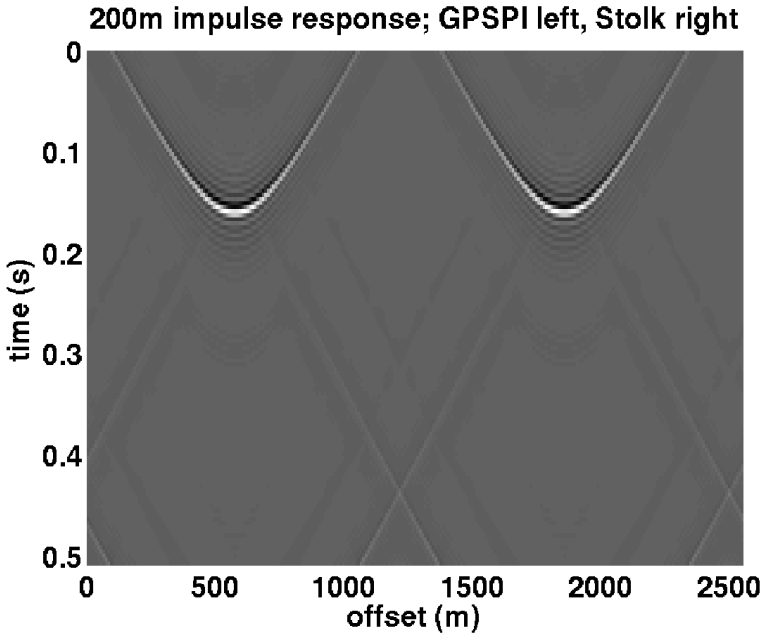

FIG. 6. Impulse response of standard symbol on the left compared to Stolk on the right, both symbols propagated an impulse 200m through a homogeneous medium.

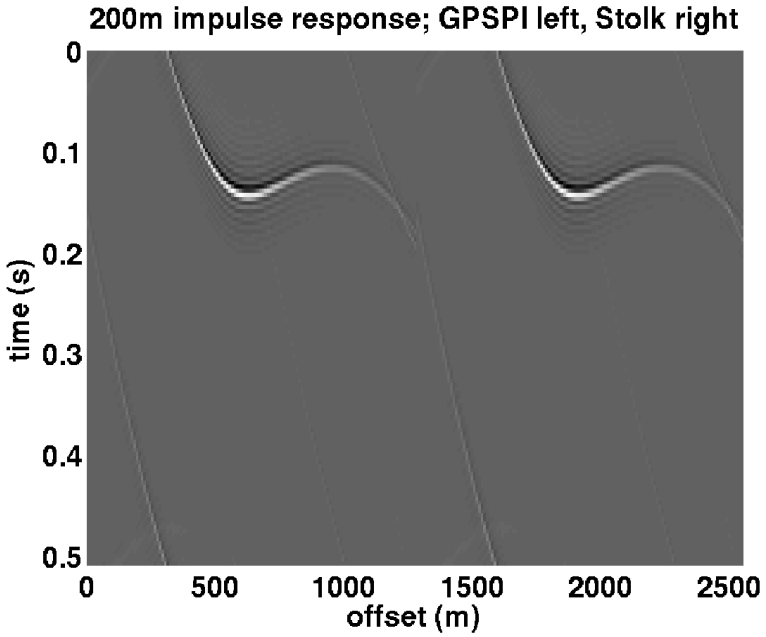

FIG. 7. Impulse response of standard symbol on the left compared to Stolk on the right, both symbols propagated an impulse 200m through a medium with a strong velocity gradient.

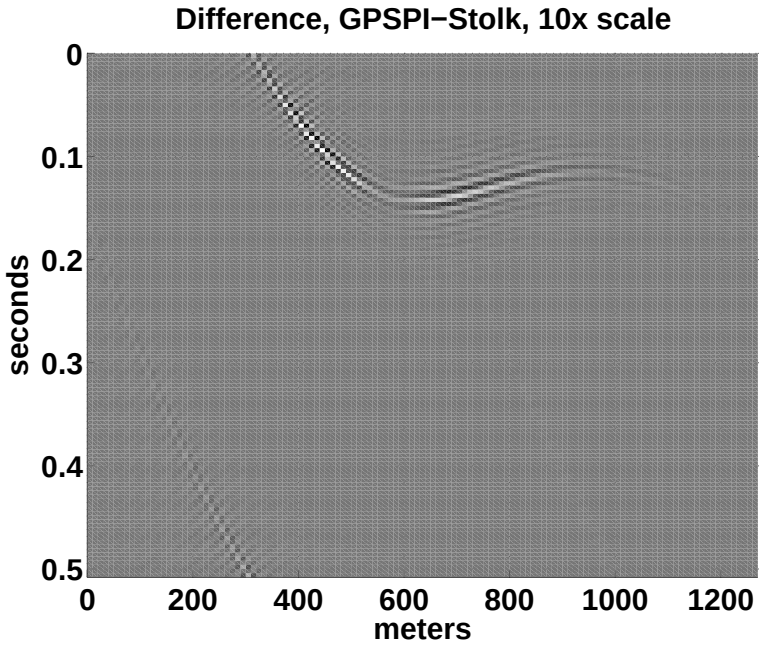

FIG. 8. Difference of standard symbol and Stolk symbol, magnified 10 times.

Focussing power

While it is interesting to observe the impulse response of the operator, the focussing power may be measured by back-propagating a wavefield that is the result of an impulse that has been forward-propagated by an exact extrapolator. In this case, the exact forward propagation was accomplished using the method of Pai (1988). After the back-propagation is executed, in principle the impulse should be recovered.

First, the "high-velocity lens" model (Figure 9) was tested. After a propagation through $200m$ with the exact extrapolator, the result was refocussed using GPSPI and Stolk operators. The resulting point is shown in Figure 10.

Visually, there is little difference between the focussing power of the two operators. Numerically there is very little difference as well. The energy density as a function of radius from the central point was measured and plotted in Figure 10. The energy density of the Stolk-focussed point is virtually indistinguishable from the GPSPI-focussed point.

A more complicated velocity model was also tested. In this case, it is a section of the Marmousi model as described by Bourgeois et al. (1991). The section used is shown in Figure 11. The resulting focussed points are compared in Figure 12, with relative energy densities compared in Figure 12. Once again, the focussing powers of the operators are very nearly identical.

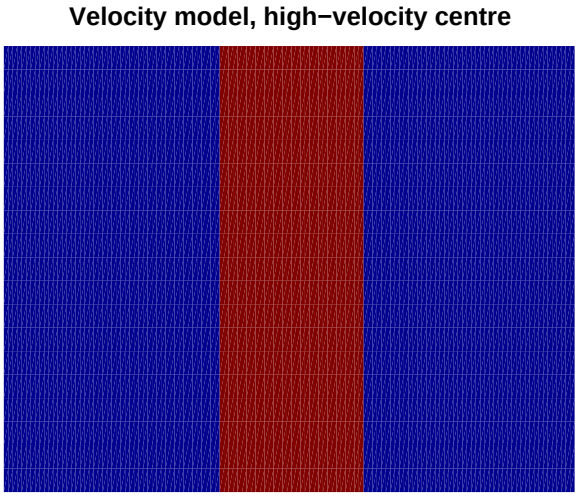

FIG. 9. High-velocity lens model. The centre is 4500 m/s, with sides at 1500 m/s. Total width of the central portion is approximately 300 m.

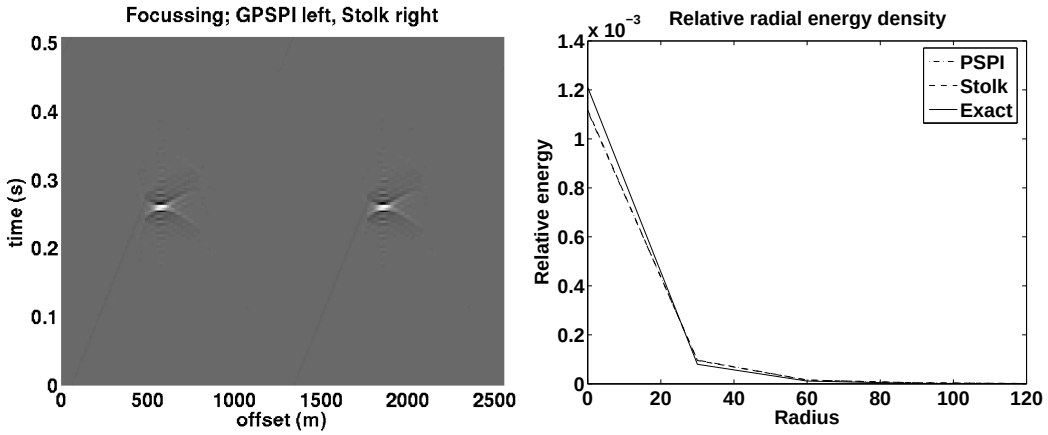

FIG. 10. Focussing power of GPSPI and Stolk operators for the high-velocity lens model on the left. Radial energy density for the high-velocity lens model on the right. The GPSPI and Stolk lines are nearly indistinguishable.

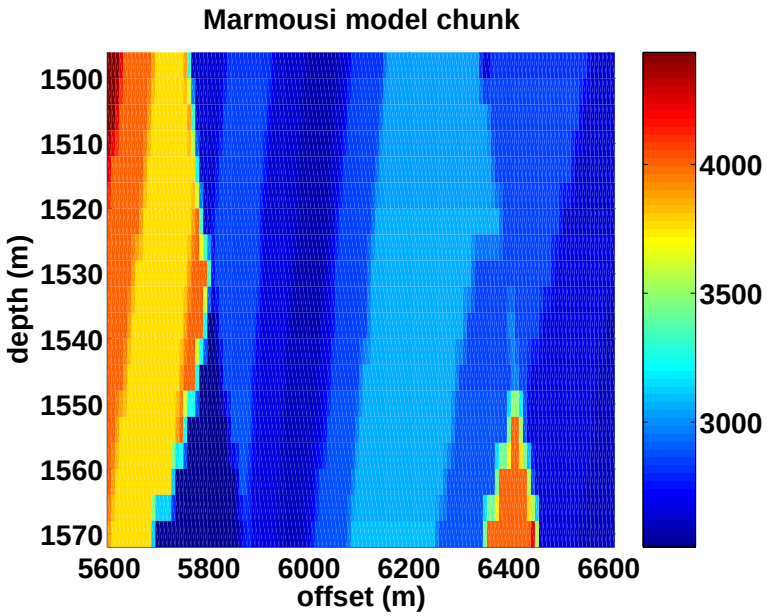

FIG. 11. Marmousi chunk model, with velocity in m/s

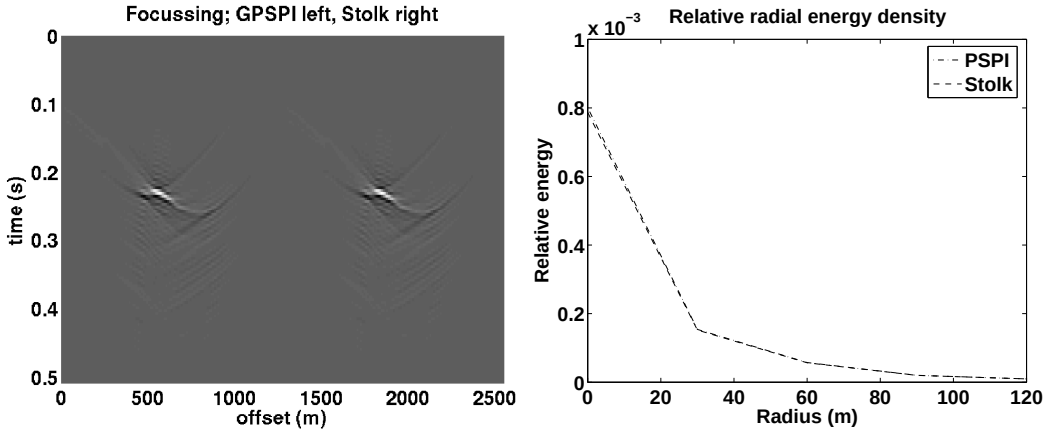

FIG. 12. Focussing power of GPSPI and Stolk operators for the Marmousi chunk model on the left. Radial energy density for the Marmousi chunk model on the right.

Marmousi migration

In addition to impulse response and focussing power tests, full prestack migrations of the Marmousi model were calculated using FOCI. The standard FOCI operator was compared to a modified version that included the Stolk correction term in the operator design phase but was otherwise identical in all operational parameters. Specifically, the operators were calculated with a forward operator size of 41 points, an inverse operator size of 51 points, and a final window size of 41 points. A standard FOCI image is shown in Figure 13, and the resulting Stolk image is shown in Figure 14. The two images are very similar.

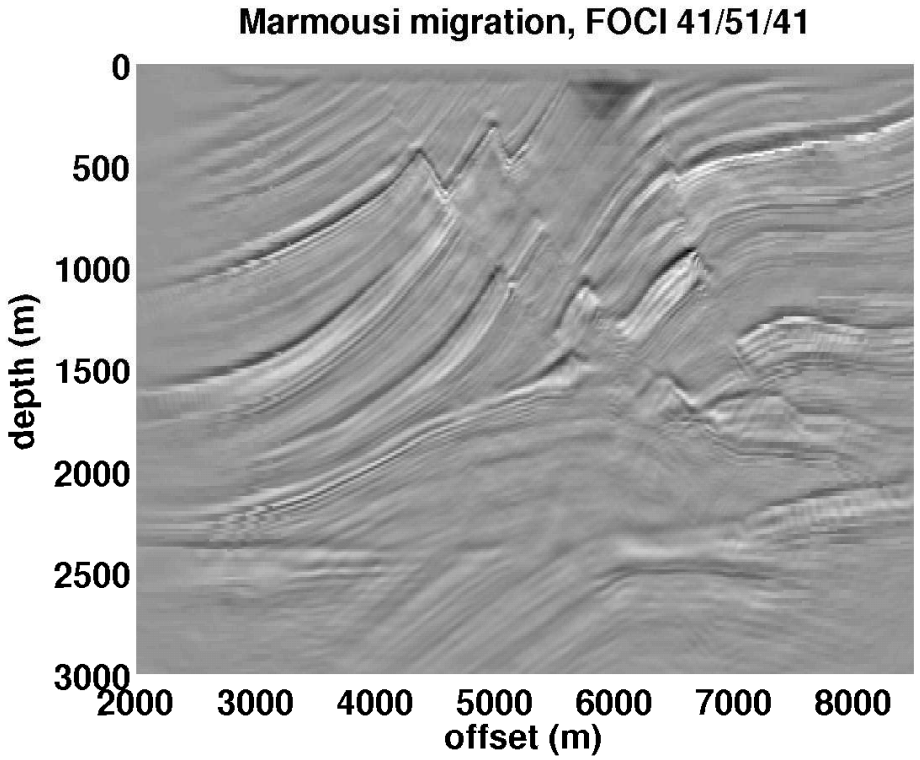

FIG. 13. Marmousi migration in standard FOCI with 41/51/41 windowing.

Several subsections of the image are compared more closely in Figures 15–18. Each figure contains four panels. On the top left, the $v(z)$ image is displayed. On the bottom left, the FOCI image is displayed. On the top right, the corresponding region from the Marmousi velocity model is displayed. On the bottom right, a histogram of the colourbar usage of both images is shown, in order to allow for an accurate comparison of the relative strengths and weaknesses of amplitudes within the images. In the first region (Figure 15) there is almost no visual difference between the two images at all. The second region (Figure 16) shows slightly better definition and continuity, especially in the neighbourhoods of $(5400, 1300)$ and $(5700, 1300)$. These differences are extremely small, however. The third region (Figure 17) reveals a very slight improvement in continuity near the top left, near $(6200, 500)$. The fourth region (Figure 18) shows perhaps slightly less definition in the Stolk image. This is evident in a small loss of resolution around $(6500, 2500)$.

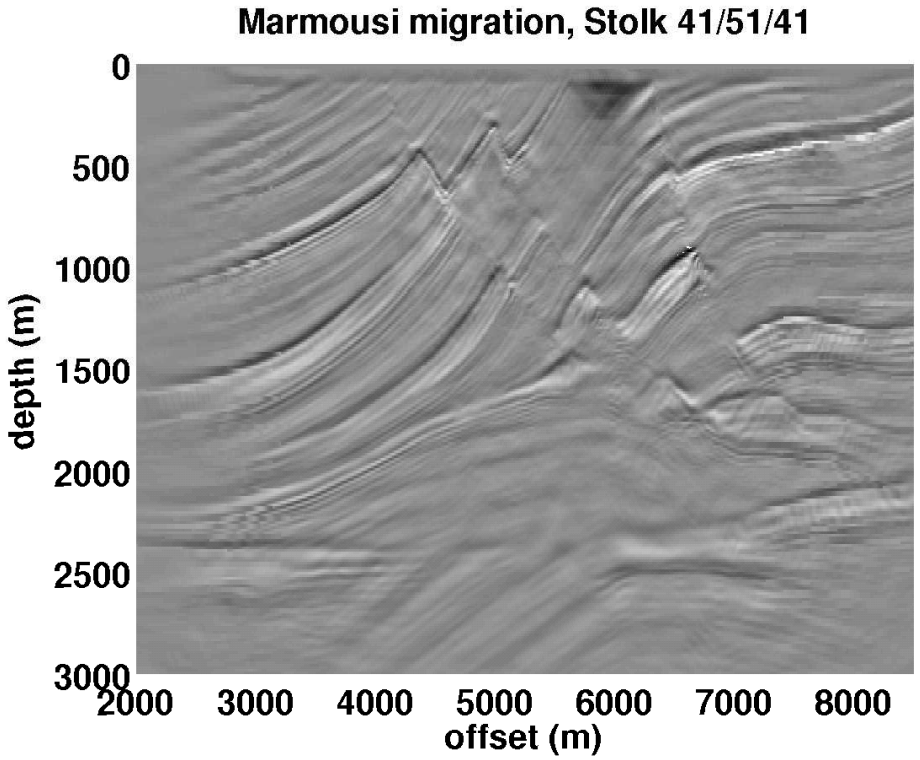

FIG. 14. Marmousi migration using Stolk correction, run with 41/51/41 windowing.

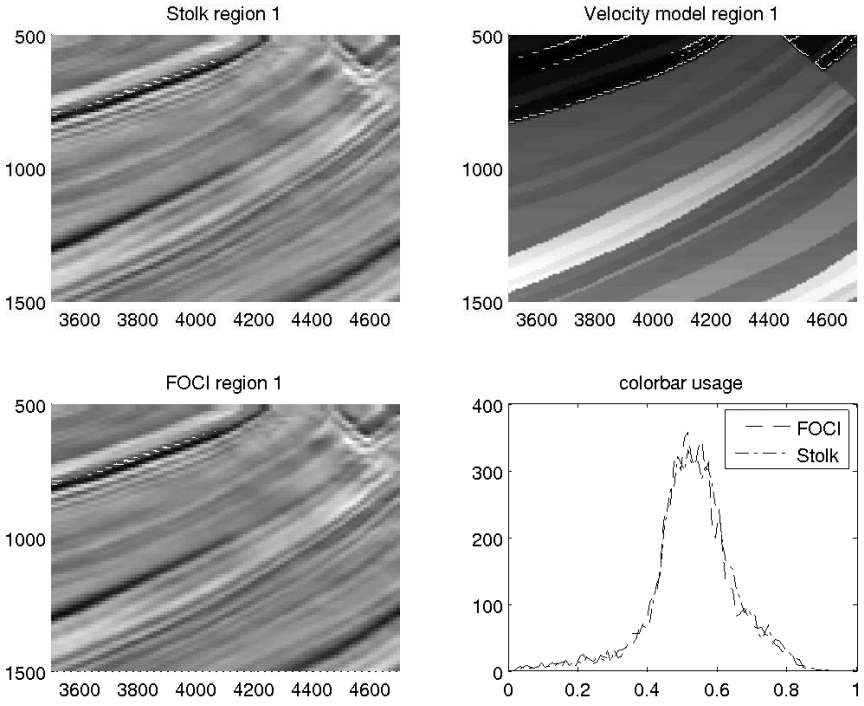

FIG. 15. Marmousi migration, Stolk vs. FOCI migration with 41/51/41 operators. Region 1.

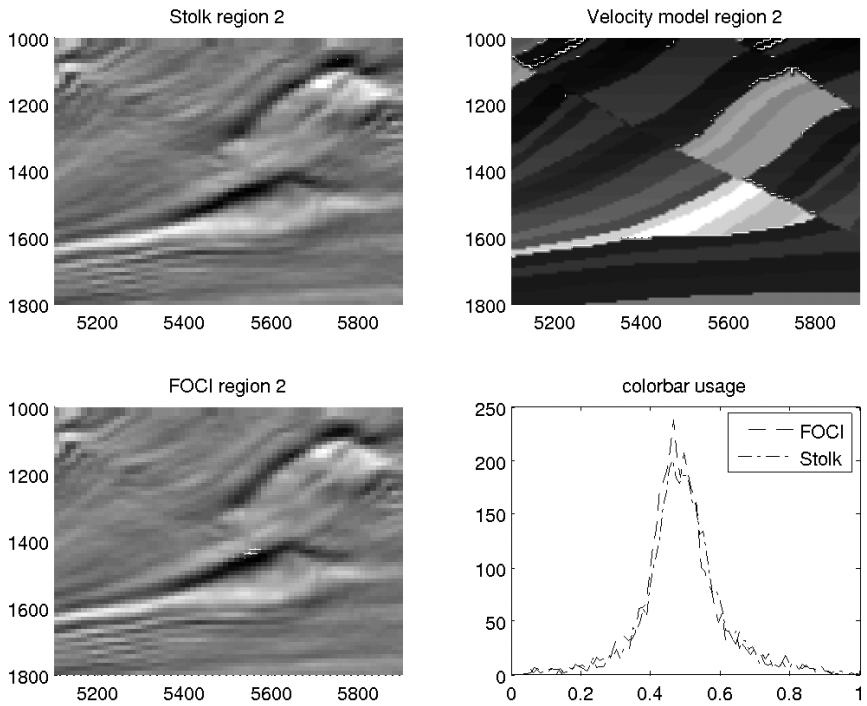

FIG. 16. Marmousi migration, Stolk vs. FOCI migration with 41/51/41 operators. Region 2.

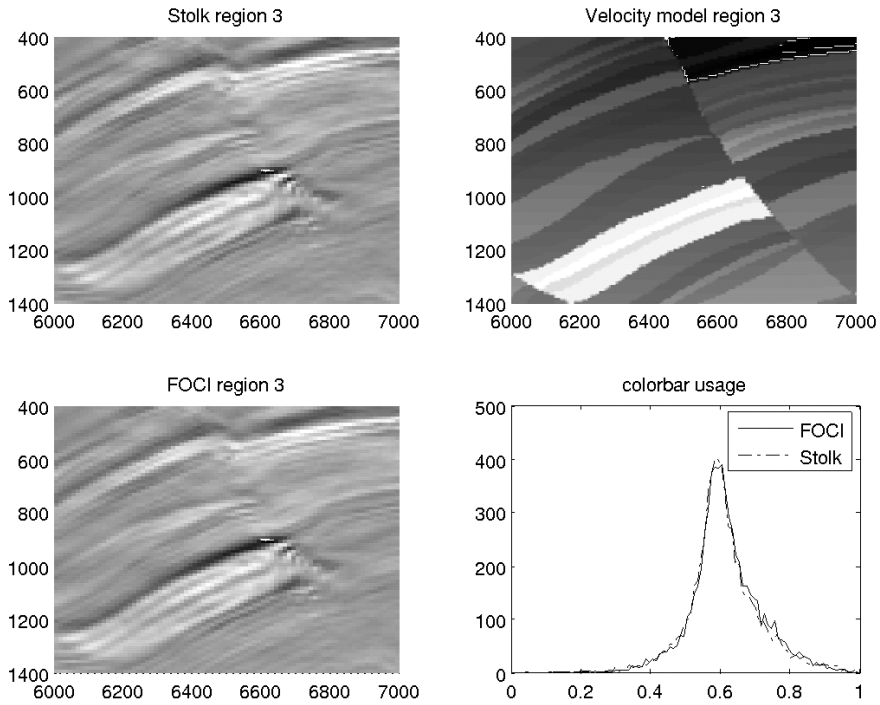

FIG. 17. Marmousi migration, Stolk vs. FOCI migration with 41/51/41 operators. Region 3.

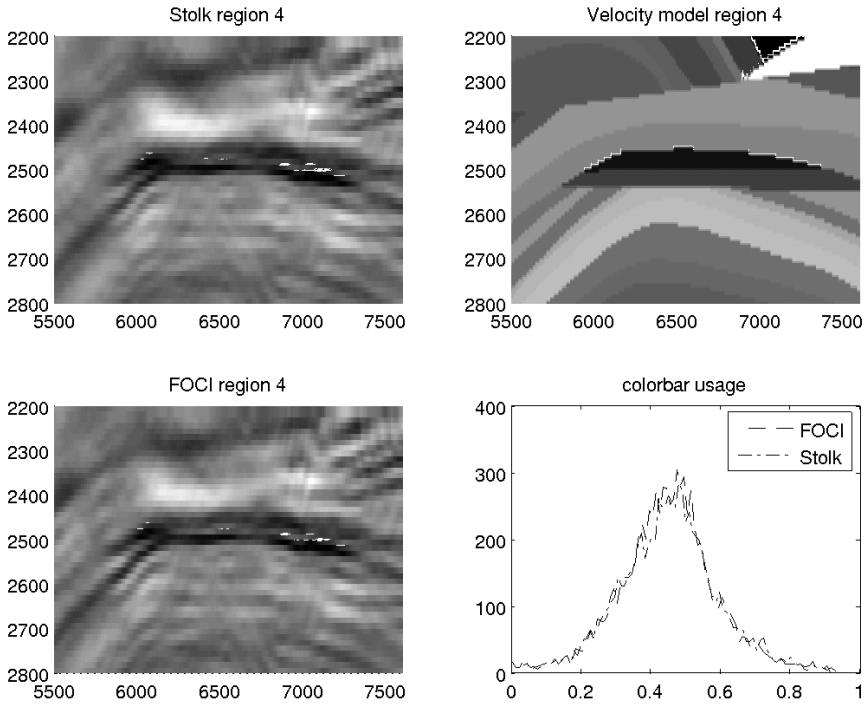

FIG. 18. Marmousi migration, Stolk vs. FOCI migration with 41/51/41 operators. Region 4.

Overall, the Stolk image seems to have the theoretical potential for better imaging, but in the migration of the Marmousi image it has produced very little actual improvement.

DISCUSSION OF IMAGING PERFORMANCE

The overall imaging performance of the Stolk operator in the migration of the Marmousi model was disappointing. It seemed to produce a very slight improvement. There were cases, however, in which the Stolk operator actually produced worse results. It was noted that performance of the Stolk operator seemed to be improved in the shallower regions, and degraded deeper down. It is possible that instabilities in the $\omega - x$ representation of the operator make it less suitable for use. This could be addressed by an alternate implementation of this method that does not make use of the FOCI algorithm, or by tuning of the FOCI algorithm as more is understood about the Stolk operator's behaviour within the FOCI framework.

Additionally, it should be noted that the Stolk correction is dependent on strong high-frequency assumptions in its derivation. The Marmousi model is not an especially high-frequency data set. We are trying to image complicated and finely-layered structures with frequencies of at most $\sim 60Hz$ with velocities between $1500ms^{-1}$ and $4500ms^{-1}$. This corresponds to wavelengths between $25m$ and $75m$ in the best case. For this structural model, a "high-frequency" assumption really only has validity in a regime where the frequencies are significantly higher than $60Hz$ if we are interested in imaging with $25m$ wavelengths

DICUSSION OF COMPUTATIONAL PERFORMANCE

All calculations were performed using MATLAB 7.1 on Linux-based PC computers with 3.06 GHz Intel Pentium 4 CPUs. The running performance of the FOCI-based Stolk migration is comparable to the running performance of standard FOCI. Standard FOCI completes the Marmousi migration in approximately 16 hours. Experience suggests that using Stolk operators adds approximately 10% more time to the imaging. The extra time is largely consumed in the overhead of selecting the correct operator from a two-dimensional table (velocity and slowness derivative) instead of just a one-dimensional (velocity only) table as for standard FOCI.

Unfortunately, the precalculation of the Stolk operators requires more computational time than the migration itself. In fact, the operator calculations require approximately 1.5 to 2 times as much calculation as the generation of the image! Standard FOCI operator calculation times are insignificant compared to the calculation time of the total image.

We believe, however, that there is significant room for improvement here. A more thorough analysis of the table calculation requirements may reveal a far more efficient manner of determining the optimal partitioning of the slowness gradient range into discrete operators. Currently, the procedure is to divide the slowness derivative dimension into the same number of elements as are contained in the velocity dimension. This procedure, combined with the substantial increase in computation time for each individual operator, makes the table calculations more than an n^2 operation. Perhaps a more sparse slowness gradient dimension would produce an adequate image, or perhaps a non-linear coverage of the slowness gradient dimension would produce an even higher quality image with less overall table computation.

Even the problem as it stands is not unmanageable, however. Once a table is calculated, it never need be calculated again (for the same parameters). Therefore, a database may store these calculations for future reuse, allowing an asymptotic approach to standard FOCI calculation times.

CONCLUSION

By incorporating the local derivative in slowness, the Stolk correction is a first step towards the inclusion of more information about the local propagation region within the GPSPI migration framework. This may eventually provide a useful imaging benefit for extremely high-frequency data sets. However, at this moment it is not clear that the benefit is worth the additional computational cost. Further research may reveal much more efficient ways to calculate and use the required operators more effectively.

REFERENCES

Bourgeois, A., Bourget, M., Lailly, P., Poulet, M., Ricarte, P., and Versteeg, R., 1991, Marmousi, model and data, *in* Proceedings of the 1990 EAEG Workshop on Practical Aspects of Seismic Data Inversion.

Fishman, L., Gautesen, A. K., and Sun, Z., 1997, Uniform high-frequency approximations of the square root Helmholtz operator symbol: Wave Motion, **26**, 127–161.

Gazdag, J., 1978, Wave equation migration with the phase-shift method: Geophysics, **43**, No. 7, 1342–1556.

Gazdag, J., and Sguazzero, P., 1984, Migration of seismic data by phase shift plus interpolation: Geophysics, **49**, No. 2, 124–131.

Hörmander, L., 1985, The Analysis of Linear Partial Differential Operators, vol. 1-4: Springer.

Margrave, G. F., 1998, Theory of nonstationary linear filtering in the Fourier domain with application to time-variant filtering: Geophysics, **63**, No. 1, 244–259.

Margrave, G. F., Al-Saleh, S. M., Geiger, H. D., and Lamoureux, M. P., 2004, The FOCI algorithm for seismic depth migration, Tech. rep., CREWES Research Report.

Margrave, G. F., and Ferguson, R. J., 1999, Wavefield extrapolation by nonstationary phase shift: Geophysics, **64**, No. 4, 1067–1078.

Pai, D. M., 1988, Generalized f-k (frequency-wavenumber) migration in arbitrarily varying media: Geophysics, **53**, No. 12, 1547–1555.

Stolk, C. C., 2004, A pseudodifferential equation with damping for one-way wave equation propagation in inhomogeneous acoustic media: Wave Motion, **40**, No. 2, 111–121.